C/NOFS observations of plasma density and electric field irregularities at post-midnight local times

W. J. Burke,[1] O. de La Beaujardière,[1] L. C. Gentile,[1] D. E. Hunton,[1] R. F. Pfaff,[2] P. A. Roddy,[1] Y.-J. Su,[1] and G. R. Wilson[1]

Received 11 May 2009; revised 1 July 2009; accepted 13 July 2009; published 19 September 2009.

[1] We report on plasma densities and electric fields measured by the C/NOFS satellite between 10 and 20 June 2008. Midway through the interval, geomagnetic conditions changed from quiescent to disturbed as a high speed stream (HSS) in the solar wind passed Earth. During the HSS passage C/NOFS encountered post-midnight irregularities that ranged from strong equatorial plasma bubbles to longitudinally broad depletions. At the leading edge of the HSS the interplanetary magnetic field rapidly intensified and rotated causing auroral electrojet currents to rise and fall within a few hours. As the electrojet relaxed, C/NOFS witnessed a rapid transition from a weakly to a strongly disturbed equatorial ionosphere that lasted ~10 hours. Eastward polarization electric fields intensified within locally depleted flux tubes. We discuss relative contributions of gravity-driven currents, overshielding electric fields and disturbance dynamos as drivers of post-midnight depletions.
Citation: Burke, W. J., O. de La Beaujardière, L. C. Gentile, D. E. Hunton, R. F. Pfaff, P. A. Roddy, Y.-J. Su, and G. R. Wilson (2009), C/NOFS observations of plasma density and electric field irregularities at post-midnight local times, *Geophys. Res. Lett.*, *36*, L00C09, doi:10.1029/2009GL038879.

1. Introduction

[2] Electromechanical forces that couple the magnetosphere-ionosphere-thermosphere (MIT) system can cause intense plasma density (δN_i) irregularities to grow in the low-latitude ionosphere. To improve understanding of irregularity formation, the Communication/Navigation Outage Forecasting System (C/NOFS) satellite was launched on 16 April 2008 into a 13° inclined orbit with apogee and perigee at ~850 and 400 km, respectively. *de La Beaujardière and C/NOFS Science Definition Team* [2003] described the mission's goals and the scientific payload designed to attain them. Here we examine δN_i variations sampled by the Planar Langmuir Probe (PLP) on C/NOFS during the solar minimum period 10–20 June 2008 when perigee was on the nightside.

[3] A striking, new feature of C/NOFS observations is the detection of deep plasma depletions at topside altitudes after local midnight. Reported irregularities appear as: (1) local depletions called equatorial plasma bubbles (EPBs) and (2) longitudinally broad, depletions that we call "plasma trenches." EPBs are magnetically field-aligned, with typical east-west dimensions of ~100 km [*Basu*, 1997] and are usually found at evening local times (LTs). Reported satellite detections of post-midnight EPBs are relatively rare [*Burke*, 1979]. Longitudinally broad (>500 km) depletions develop in the evening sector during the main phases of large magnetic storms when the peak of the F-layer rises above the spacecraft [*Greenspan et al.*, 1991]. C/NOFS has detected similar phenomena at post-midnight local times under much less stressful geomagnetic conditions.

[4] EPBs begin as small-amplitude irregularities at bottomside altitudes then intensify via a generalized Rayleigh-Taylor (R-T) instability [*Balsley et al.*, 1972; *Ott*, 1978]. Forces driving the R-T instability include gravity-driven currents [*Eccles*, 2004] and quasi-DC electric fields ($\mathbf{E_0}$) with eastward components. The main sources of eastward components in the dusk sector are: (1) solar quiet (*Sq*) current system interactions with conductivity gradients near sunset, and (2) penetration electric fields from high latitudes. Polarization electric fields (E_P) can be much larger than E_0, allowing bubbles to percolate through the topside at high speeds. Inside trenches E_0 may dominate. Our analysis utilizes simultaneous measurements of plasma densities by the planar Langmuir probe (PLP) and the Vector Electric Field Instrument (VEFI) [*de La Beaujardière and C/NOFS Science Definition Team*, 2003] observed in and near irregularities. VEFI measures the total electric field's east-west (E_{zonal}) component that includes E_0 and E_P. During brief intervals when VEFI's pre-amplifiers were subject to oscillations data outputs do not reflect geophysical conditions and are not plotted.

[5] The systematics of background E_{zonal} at low latitudes have been inferred from plasma flows detected by satellites [*Fejer et al.*, 2008] and from incoherent backscatter radar measurements [*Scherliess and Fejer*, 1997]. Vertical drifts caused by eastward electric fields ($E_{zonal} > 0$) are characterized by pre-reversal enhancements (PREs) near the dusk terminator. At post-sunset LTs plasma initially rises in response to polarization charges [*Farley et al.*, 1986]; and/or Sq current diversions [*Haerendel and Eccles*, 1992] near the terminator. After ~20:00 LT the direction of the vertical drift usually reverses, stabilizing the bottomside F-layer against irregularity growth. E_{zonal} normally remains westward across the nightside. Thus the PRE opens windows of opportunity for EPBs to form before damping dominates. PRE intensities have seasonal, longitudinal, and solar cycle dependencies, tending to be largest near solar-maximum equinoxes [*Scherliess and Fejer*, 1997]. At solar minimum PRE drifts are weak.

[6] Mechanisms responsible for post-midnight $E_{zonal} > 0$ at low latitudes include: (1) dusk-to-dawn, overshielding electric fields that appear in the recovery phases of storms

[1]Space Vehicles Directorate, Air Force Research Laboratory, Hanscom, AFB, Massachusetts, USA.
[2]NASA Goddard Space Flight Center, Greenbelt, Maryland, USA.

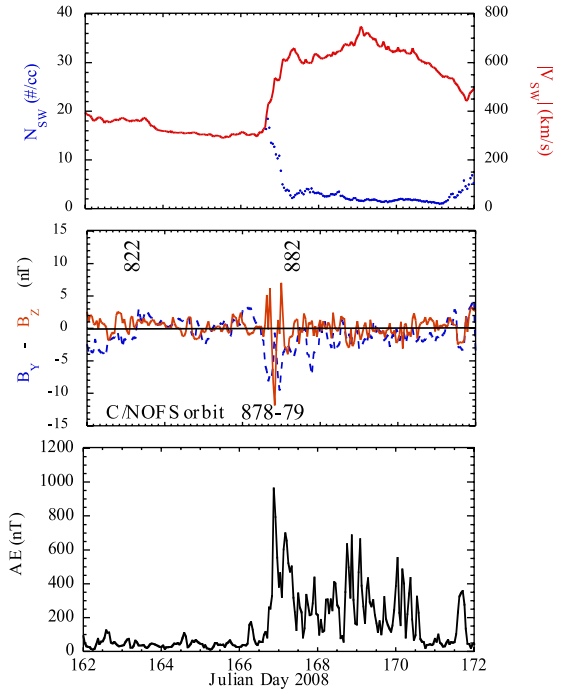

Figure 1. Interplanetary and auroral electrojet activity between 10 and 20 June 2008, including: solar wind densities (blue) and speeds (red) measured near (top) L_1, (middle) IMF B_Y (blue) and B_Z (red), and (bottom) the AE index.

and substorms [*Kikuchi et al.*, 2000, 2008] while Region 2 remain relatively strong, and (2) disturbance dynamos excited by Poynting and energetic particle fluxes into the auroral ionosphere [*Blanc and Richmond*, 1980; *Fejer and Scherliess*, 1995, 1997; *Scherliess and Fejer*, 1997]. *Blanc and Richmond* [1980] argued that heating at high latitudes drives equatorward winds. Associated equatorward Pedersen currents accumulate polarization charges at mid latitudes that drive plasma circulation in the anti-Sq sense with equatorial electric fields having eastward (westward) components on the nightside (dayside). *Fejer and Scherliess* [1995] demonstrated agreement between the LT distributions of radar measured vertical drifts and the model predictions. C/NOFS detections of post-midnight EPBs provide opportunities to weigh contributions of these mechanisms for producing $E_{zonal} > 0$ on the nightside. In principle, disturbance dynamo E_{zonal} produces relatively sustained increases in post-midnight EPB activity beginning a few hours after the disturbance onset and lasting up to 30 hours after they abate [*Scherliess and Fejer*, 1997]. Overshielding fields occur early in recovery while Region 2 currents relax at slower rates than those of Region 1 [*Kikuchi et al.*, 2000].

2. Observations

[7] Figure 1 summarizes interplanetary conditions observed by the Advanced Composition Explorer (ACE) satellite and induced geomagnetic responses during 10–20 June 2008 (Julian Days 162–172). The top plot shows solar wind densities N_{SW} (blue) and speeds V_{SW} (red) from measurements by the Solar Wind Electron Proton and Alpha Monitor [*McComas et al.*, 1998]. The second shows the interplanetary magnetic field (IMF), GSM B_Y (blue) and B_Z (orange) components measured by the Magnetic Field Instrument [*Smith et al.*, 1998]. The bottom plot is the AE index. While quantities in Figure 1 are hourly averages, our analyses use higher resolution data.

[8] On JD 166, V_{SW} rose from ~310 km/s at 16:00 UT to 640 km/s and remained >600 km/s though JD 170. N_{SW} data are unavailable prior to 15:36 UT on JD 166. As V_{SW} increased, N_{SW} first rose to 18.6 then fell to about 2 cm^{-3}. Combined N_{SW}-V_{SW} variations near 17:00 UT indicate that a corotating interaction region (CIR) formed at the leading edge of the HSS [*Balogh et al.*, 1999; *Tsurutani et al.*, 2006]. The IMF was weak both before V_{SW} increased and inside the HSS. Within the CIR transverse IMF components reached ~12 nT then rotated from northwest to south to northwest. From JD 162 to 166.5 AE was low 44.6 ± 24.3 nT with weak events excited by brief southward excursions. AE responded strongly to IMF turnings in the CIR and HSS. Peak excursions of 1311 and 1030 nT occurred at 21:27 UT on JD 166 and at 03:55 UT on JD 167, respectively. It remained high but erratic (237.0 ± 184.5 nT) as the HSS passed Earth.

[9] C/NOFS data are considered in two stages with N_i and E_{zonal} reported at 1-s cadences. Figure 2 shows N_i measurements from consecutive orbits near the CIR impact. Figure 3 contains N_i and E_{zonal} measurements representative nightside passes before and during the HSS passage. Unsurprisingly, N_i and E_{zonal} variations anti-correlate in regions of plasma irregularities. Before examining C/NOFS data it is useful to consider orbital constraints that influence interpretations. On 10 June C/NOFS' perigee and ascending node were near 01:00 and 19:00 LT. The ascending node's longitude progresses ~24.2° to the west on successive orbits. C/NOFS thus provides 3 to 4 snapshots of the nightside ionosphere at a given longitude, albeit at different latitudes and altitudes. Orbital lines of apsides and nodes precessed ~7.5° to the east and ~8.25° to the west per day, respectively. C/NOFS approached perigee after local midnight. Locations of the ascending node and perigee placed C/NOFS north of the geographic equator at nightside LTs. Perigee was near the magnetic equator in the African to central Pacific sector but at Appleton anomaly magnetic latitudes at eastern Pacific to South American longitudes.

[10] Figure 2 shows N_i measurements from late on 14 June. Double arrows mark the durations of C/NOFS orbits 878 and 879. The letters M and P mark midnight and perigee crossings. Horizontal bars span periods when

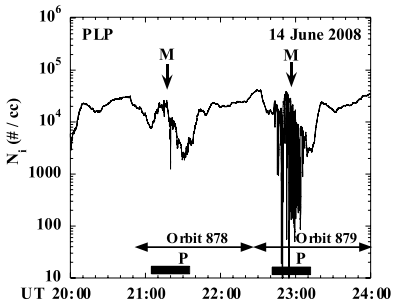

Figure 2. PLP plasma densities measured between 20:00 and 24:00 UT on 14 June 2008. Times of C/NOFS orbits 878 and 879 are indicated along with midnight meridian (M) and perigee (P) crossings. Solid bars mark intervals when C/NOFS was in darkness.

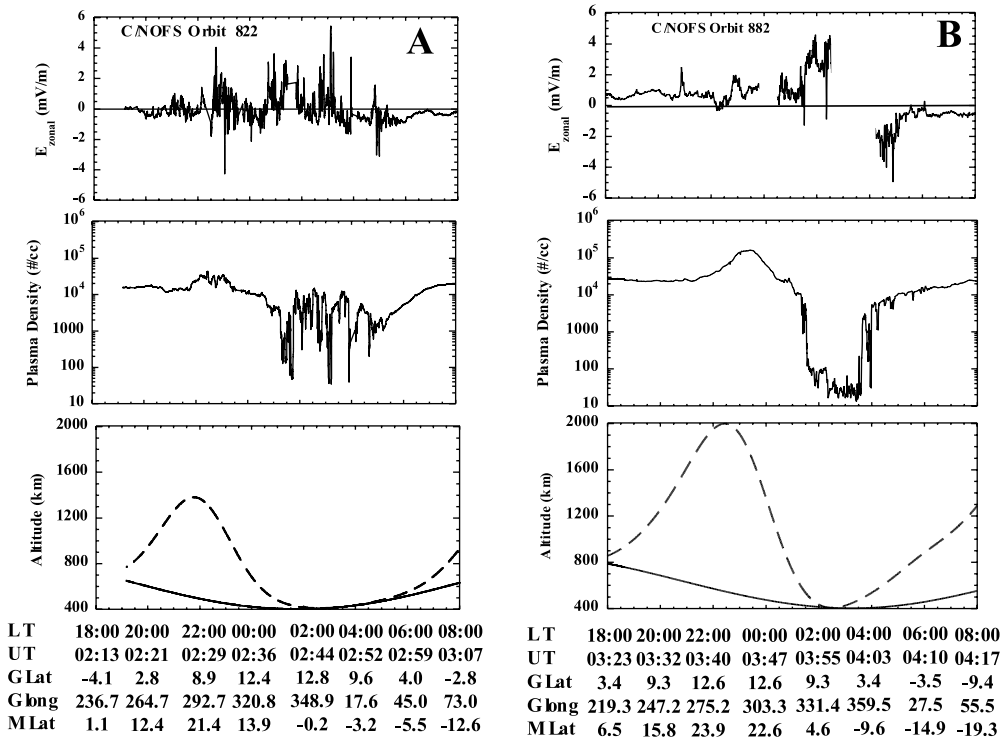

Figure 3. (top) Zonal electric fields and (middle) plasma densities measured by C/NOFS during orbits (a) 822 and (b) 882, plotted as functions of LT, UT, geographic latitude, geographic longitude, and geomagnetic latitude. Orbit 822 illustrates predisturbance conditions; orbit 882 occurred shortly after the CIR passage. (bottom) Traces indicate geographic altitudes (solid lines) of C/NOFS and the apex altitudes of magnetic field lines on which measurements were made.

C/NOFS was in darkness. During the eclipsed portions of orbits 878 and 879 C/NOFS crossed longitudes $-10°$ to 105°E and $-35°$ to 80°E, respectively. Thus, both passes covered African to Indian Ocean longitudes. Except for one depletion near 21:20 UT (00:45 LT, ~50°E) δN_i amplitudes were small during orbit 878. Conversely, on orbit 879 C/NOFS encountered continuous large $\delta N_i/N_i >$ 100 irregularities from eastern Atlantic through African longitudes. Pre-midnight EPBs apparent on orbit 879 are singular exceptions to the post-midnight rule for these ten days. Expanded views of N_i (not given) indicate that local δN_i depressions were 110 to 480 km wide. The African sector is common to both observations. Thus, differences observed between orbit 878 and 879 are time dependent. Note that the first AE peak occurred ~1 hour before the start of orbit 879.

[11] Figure 3 shows E_{zonal} (Figure 3, top) and N_i (Figure 3, middle) sampled at similar longitudes during C/NOFS orbits 822 (Figure 3a) and 882 (Figure 3b). These data were acquired during the magnetically quiet/disturbed JD 163/167, respectively and are plotted as functions of LT beginning at ascending nodes, UT, geographic latitude (GLat), geographic longitude (GLong) and corrected magnetic latitude (MLat). The bottom plots indicate spacecraft altitudes (solid lines) and apex altitudes of magnetic field lines (dashed lines). Traces converge where C/NOFS was near the magnetic equator.

[12] Plasma densities shown in Figure 3a increased at pre-midnight LTs as the C/NOFS altitude decreased. Evening sector irregularities appear as weak local increases and decreases. Starting at ~23:00 LT while C/NOFS was descending, N_i decreased gradually. After local midnight N_i fell precipitously near perigee. From ~01:00 LT through dawn C/NOFS crossed a series of (factors of 10 to 100) EPB depletions; E_{zonal} was irregular and eastward within the depletions. C/NOFS remained close to the magnetic equator as its trajectory rose from perigee. Figure 3b (middle) shows a pre-midnight N_i enhancement followed by post-midnight irregularities and depletions, but EPB signatures were infrequent. Rather, C/NOFS crossed a wide (~3500 km) plasma density trench from ~03:53 to 04:01 UT (01:45-04:00 LT) on JD 167. Across this deep depletion, the average E_{zonal} was ~2.4 mV/m eastward (Figure 3b, top). After 03:56:15 UT, (~02:30 LT) when the plasma density abruptly fell to ~20 cm^{-3}, E_{zonal} variations increased dramatically but with no correspondence to simultaneous changes in measured δNi. At these low densities the Debye length grew to ~1 m. Thus, observed E_{zonal} fluctuations probably reflect responses to differences in VEFI's sheath impedances. We note, but do not show, that the large-amplitude irregularities of orbit 879 appear to have evolved into the broad trench. During nightside parts of orbits 880 and 881, C/NOFS encounters with topside plasma diminished and the longitudinal scale sizes of N_i depletions widened. The deep depletion of orbit 882 narrowed during orbit 883 then disappeared as the affected ionosphere rotated into the dayside.

[13] Data acquired during nightside passes of Figure 3 also illustrate relationships between N_i (blue) and E_{zonal} (red). During orbit 822 δN_i and δE_{zonal} strongly anti-correlated, E_{zonal} intensified within N_i depletions. This is consistent with C/NOFS' passing through upwelling EPBs permeated by

strong polarization electric fields [*Ott*, 1978]. This relationship continued during orbit 882, from 03:54–03:55 UT, while C/NOFS was in the western part of the deep plasma trench. However, at ~03:56:13 UT as N_i rapidly decreased from to ~15 cm^{-3}, δE_{zonal} underwent large amplitude oscillations related to large sheaths around VEFI. The quasi DC portion of E_{zonal} was ~2.4 mV/m across the orbit 882 plasma trench, consistent with the local F layer being lifted above C/NOFS.

3. Discussion

[14] This study focused on dynamics of the nightside, equatorial ionosphere before and during passage of a HSS in the solar wind. During this period C/NOFS' perigee was at post-midnight LTs. Interplanetary and AE data show three distinct intervals, (1) geomagnetic quiet, JD 162–166.5, (2) responses to the CIR magnetic field rotation JD 166.5–167, and (3) HSS induced activity JD 167–170.

[15] Figure 3a (middle) shows that from the western Atlantic across Africa to the central Pacific (~160°E) C/NOFS detected pre-disturbance EPBs and large depletions after midnight. At other longitudes C/NOFS was away from the magnetic equator. Even during sustained periods of magnetic quiet in solar minimum bottomside irregularities grew into EPBs. This raises a question. What mechanism supports the development of EPBs at post-midnight LTs during quiet intervals when neither overshielding nor disturbance dynamo E_{zonal} fields can operate? Solar UV fluxes driving dayside dynamos and consequent PRE signatures were also weak. With no post-dusk westward E_{zonal} to stabilize the bottomside ionosphere, the gravitational drift current $j_G = n_i(m_i\mathbf{g} \times \mathbf{B})/B^2$ has no competitors. Normally insufficient time is available for j_G to drive bottomside irregularities into the nonlinear regime before E_{zonal} turns westward [*Basu*, 1997]. If $E_{zonal} \approx 0$, data suggest that enough time becomes available for EPBs to grow and reach altitudes $\geq$400 km after midnight.

[16] Figure 2 shows that the nightside ionosphere responded to the CIR passage. Except for the high number of EPBs encountered during orbit 879 the upper envelopes of N_i traces for orbits 878 and 879 were similar. The R-T growth rate equation [*Ott*, 1978] suggests that an eastward E_{zonal} was present on the nightside during the hour before C/NOFS orbit 879. AE first peaked at 21:27 UT then decreased at a rate of 283 nT/hr. *Scherliess and Fejer* [1997] estimated that several hours are needed for disturbance-dynamo effects to reach the equator. On the other hand, overshielding electric fields appear soon after the IMF turns northward [*Kikuchi et al.*, 2000]. We suggest that overshielding was primarily responsible for changes seen between orbits 878 and 879.

[17] During orbit 882 C/NOFS crossed a broad and deep depletion with average $E_{zonal} \approx 2.4$ mV/m. With an equatorial magnetic field of ~31,000 nT, this corresponds to upward drifts of ~77 m/s. It would take ~22 minutes for the F layer to rise 100 km. Thus, within this deep trench C/NOFS sampled plasma that originated far below the peak height of the quiescent F layer. Between JD 167 and 170 C/NOFS witnessed several cycles of plasma and AE quieting and activation. With available information it is difficult to distinguish between overshielding and disturbance-dynamo contributions. However, the average $E_{zonal} \approx 2.4$ mV/m measured across the deep plasma trench seems to be a disturbance dynamo effect. Early on JD 167 the downward trend of AE reversed, reaching a second peak of 1030 nT at 03:55 UT. It appears unlikely that an overshielding E_{zonal} operated in the hour prior to orbit 882. Within the bounds of present understanding only the disturbance dynamo can explain the strong eastward E_{zonal} measured during orbit 882.

4. Conclusions

[18] This study of C/NOFS measurements indicates that during June 2008 EPBs and deep plasma trenches formed at post-midnight LTs. These features were present during an extended period of magnetic quiet, but intensified after the CIR's coupling to the magnetosphere-ionosphere weakened and allowed the auroral electrojet to relax. Observed EPB activity waxed and waned as the HSS passed Earth. Our analysis supports four conclusions:

[19] 1. Active post-midnight EPBs carry eastward polarization electric fields and indicate that irregularities can form and reach C/NOFS altitudes even during magnetically quiet intervals in solar minimum. Under these conditions $n_i m_i(\mathbf{g} \times \mathbf{B})$ currents acquire sufficient time to drive nonlinear R-T instabilities.

[20] 2. Intensification of EPB activity, observed about an hour after the CIR-induced peak in AE, was probably caused by eastward overshielding electric fields.

[21] 3. The plasma trench of orbit 882 with $E_{zonal} \approx$ 2.4 mV/m was observed while AE was increasing and thus appears to be mostly a disturbance dynamo effect.

[22] 4. Continued, albeit sporadic, detections of EPBs and plasma trenches during the four days of the HSS passage suggest that both overshielding and disturbance dynamos remained active. Presently available information is insufficient to distinguish their distinctive contributions.

[23] **Acknowledgments.** The C/NOFS mission is supported by the Air Force Research Laboratory, the Department of Defense Space Test Program, the National Aeronautics and Space Administration, the Naval Research Laboratory, and the Aerospace Corporation. This analysis was supported by Air Force Office of Scientific Research Task 2301SDA5 and Air Force contract FA8718-08-C-0012 with Boston College.

References

Balogh, A., J. T. Gosling, J. R. Jokipii, R. Kallenbach, and H. Kunow (Eds.) (1999), Corotating interaction regions, *Space Sci. Rev.*, *89*, 141, doi:10.1023/A:1005245306874.

Balsley, B. B., G. Haerendel, and R. A. Greenwald (1972), Equatorial spread F: Recent observations and a new interpretation, *J. Geophys. Res.*, *77*, 5625, doi:10.1029/JA077i028p05625.

Basu, B. (1997), Generalized Rayleigh-Taylor instability in the presence of time-dependent equilibrium, *J. Geophys. Res.*, *102*, 17,305, doi:10.1029/97JA01239.

Blanc, M., and A. D. Richmond (1980), The ionospheric disturbance dynamo, *J. Geophys. Res.*, *85*, 1669, doi:10.1029/JA085iA04p01669.

Burke, W. J. (1979), Plasma bubbles near the dawn terminator in the topside ionosphere, *Planet. Space Sci.*, *27*, 1187, doi:10.1016/0032-0633(79)90138-7.

de La Beaujardière, O., and C/NOFS Science Definition Team (2003), Communication/Navigation Outage Forecasting System (C/NOFS) science plan, *Rep. AFRL/VS-TR-2003-1501*, Air Force Res. Lab., Hanscom AFB, Mass.

Eccles, J. V. (2004), The effect of gravity and pressure in the electrodynamics of the low-latitude ionosphere, *J. Geophys. Res.*, *109*, A05304, doi:10.1029/2003JA010023.

Farley, D., E. Bonelli, B. Fejer, and M. Larsen (1986), The prereversal enhancement of the zonal electric field in the equatorial ionosphere, *J. Geophys. Res.*, *91*, 13,723, doi:10.1029/JA091iA12p13723.

Fejer, B. G., and L. Scherliess (1995), Time dependent response of equatorial ionospheric electric fields to magnetospheric disturbances, *Geophys. Res. Lett.*, *22*, 851, doi:10.1029/95GL00390.

Fejer, B. G., and L. Scherliess (1997), Empirical models of storm time equatorial zonal electric fields, *J. Geophys. Res.*, *102*, 24,047, doi:10.1029/97JA02164.

Fejer, B. G., J. W. Jensen, and S.-Y. Su (2008), Quiet time equatorial F region plasma drift model derived from ROCSAT observations, *J. Geophys. Res.*, *113*, A05304, doi:10.1029/2007JA012801.

Greenspan, M. E., C. E. Rasmussen, W. J. Burke, and M. A. Abdu (1991), Equatorial density depletions observed at 840 km during the great magnetic storm of March 1989, *J. Geophys. Res.*, *96*, 13,931, doi:10.1029/91JA01264.

Haerendel, G., and J. V. Eccles (1992), The role of the equatorial electrojet in the evening ionosphere, *J. Geophys. Res.*, *97*, 1181, doi:10.1029/91JA02227.

Kikuchi, T., H. Lühr, K. Schlegel, H. Tachihara, and T.-I. Kitamura (2000), Penetration of auroral electric fields to the equator during a substorm, *J. Geophys. Res.*, *105*, 23,251, doi:10.1029/2000JA900016.

Kikuchi, T., K. K. Hashimoto, and K. Nozaki (2008), Penetration of magnetospheric electric fields to the equator during geomagnetic storms, *J. Geophys. Res.*, *113*, A06214, doi:10.1029/2007JA012628.

McComas, D. J., S. J. Bame, P. Barber, W. C. Fieldman, J. L. Phillips, and P. Riley (1998), Solar wind electron, proton, and alpha monitor (SWEPAM) on the Advanced Composition Explorer, *Space Sci. Rev.*, *86*, 563, doi:10.1023/A:1005040232597.

Ott, E. (1978), Rayleigh-Taylor bubbles in the equatorial ionosphere, *J. Geophys. Res.*, *83*, 2066, doi:10.1029/JA083iA05p02066.

Scherliess, L., and B. G. Fejer (1997), Storm time dependence of equatorial disturbance dynamo zonal electric fields, *J. Geophys. Res.*, *102*, 24,037, doi:10.1029/97JA02165.

Smith, C. W., M. H. Acuña, L. F. Burlaga, J. L. L'Heureux, N. F. Ness, and J. Scheifele (1998), The ACE magnetic field experiment, *Space Sci. Rev.*, *86*, 613, doi:10.1023/A:1005092216668.

Tsurutani, B. T., et al. (2006), Corotating solar wind streams and recurrent geomagnetic activity: A review, *J. Geophys. Res.*, *111*, A07S01, doi:10.1029/2005JA011273.

W. J. Burke, O. de La Beaujardière, L. C. Gentile, D. E. Hunton, P. A. Roddy, Y.-J. Su, and G. R. Wilson, Space Vehicles Directorate, Air Force Research Laboratory, 29 Randolph Road, Hanscom AFB, MA 01731-3010, USA. (afrl.rvb.pa@hanscom.af.mil)

R. F. Pfaff, NASA Goddard Space Flight Center, Mail Code 674, Greenbelt, MD 20771, USA.